

AD-A147 561

THE CHARGE-STATE COMPOSITION OF 04-MEV HELIUM IONS IN
EARTH'S OUTER RADIA. (U) AEROSPACE CORP EL SEGUNDO CA
SPACE SCIENCES LAB D L CHENETTE ET AL. 30 SEP 84

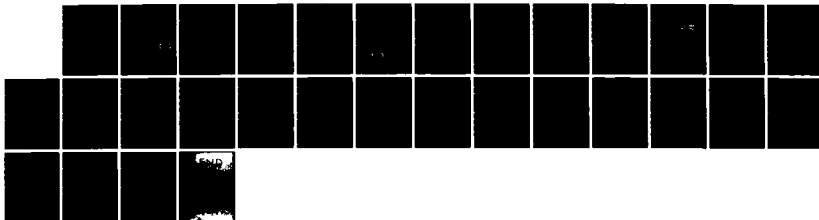
1/1

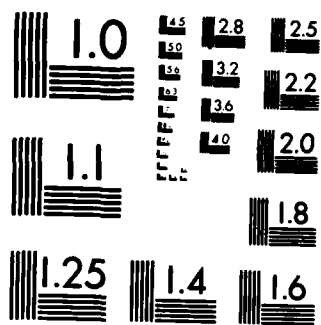
UNCLASSIFIED

TR-0084(4940-05)-06 SD-TR-84-48

F/G 4/1

NL





12

The Charge-State Composition of 0.4-MeV Helium Ions in Earth's Outer Radiation Belts during Quiet Times

D. L. CHENETTE, J. B. BLAKE, and J. F. FENNELL
Space Sciences Laboratory
Laboratory Operations
The Aerospace Corporation
El Segundo, Calif. 90245

30 September 1984

DTIC
ELECTE
NOV 16 1984
S B

APPROVED FOR PUBLIC RELEASE;
DISTRIBUTION UNLIMITED

Prepared for
SPACE DIVISION
AIR FORCE SYSTEMS COMMAND
Los Angeles Air Force Station
P.O. Box 92960, Worldway Postal Center
Los Angeles, Calif. 90009

84 11 13 042

AD-A147 561

FILE COPY

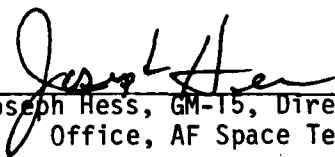
This report was submitted by The Aerospace Corporation, El Segundo, CA 90245, under Contract No. F04701-83-C-0084 with the Space Division, P.O. Box 92960, Worldway Postal Center, Los Angeles, CA 90009. It was reviewed and approved for The Aerospace Corporation by H. R. Rugge, Director, Space Sciences Laboratory. 1st Lt. Douglas R. Case, SD/YCM, was the project officer for the Mission-Oriented Investigation and Experimentation (MOIE) program.

This report has been reviewed by the Public Affairs Office (PAS) and is releasable to the National Technical Information Service (NTIS). At NTIS, it will be available to the general public, including foreign nationals.

This technical report has been reviewed and is approved for publication. Publication of this report does not constitute Air Force approval of the report's findings or conclusions. It is published only for the exchange and stimulation of ideas.



Douglas R. Case, 1st Lt, USAF
Project Officer



Joseph Hess, GM-15, Director, West Coast
Office, AF Space Technology Center

UNCLASSIFIED

SECURITY CLASSIFICATION OF THIS PAGE (When Data Entered)

REPORT DOCUMENTATION PAGE		READ INSTRUCTIONS BEFORE COMPLETING FORM
1. REPORT NUMBER SD-TR-84-48	2. GOVT ACCESSION NO.	3. RECIPIENT'S CATALOG NUMBER
4. TITLE (and Subtitle) THE CHARGE-STATE COMPOSITION OF 0.4-MeV HELIUM IONS IN EARTH'S OUTER RADIATION BELTS DURING QUIET TIMES		5. TYPE OF REPORT & PERIOD COVERED
7. AUTHOR(s) David L. Chenette, J. Bernard Blake, and Joseph F. Fennell		6. PERFORMING ORG. REPORT NUMBER TR-0084(4940-05)-06
9. PERFORMING ORGANIZATION NAME AND ADDRESS The Aerospace Corporation El Segundo, Calif. 90245		8. CONTRACT OR GRANT NUMBER(s) F04701-83-C-0084
11. CONTROLLING OFFICE NAME AND ADDRESS Space Division Los Angeles Air Force Station Los Angeles, Calif. 90009		10. PROGRAM ELEMENT, PROJECT, TASK AREA & WORK UNIT NUMBERS
14. MONITORING AGENCY NAME & ADDRESS (if different from Controlling Office)		12. REPORT DATE 30 September 1984
		13. NUMBER OF PAGES 24
		15. SECURITY CLASS. (of this report) Unclassified
		15a. DECLASSIFICATION DOWNGRADING SCHEDULE
16. DISTRIBUTION STATEMENT (of this Report) Approved for public release; distribution unlimited.		
17. DISTRIBUTION STATEMENT (of the abstract entered in Block 20, if different from Report)		
18. SUPPLEMENTARY NOTES		
19. KEY WORDS (Continue on reverse side if necessary and identify by block number) Charge-state Magnetosphere Composition Radiation Environment Techniques Geosynchronous orbit Trapped particles Helium		
20. ABSTRACT (Continue on reverse side if necessary and identify by block number) > We present measurements of the charge state of 0.40 - 0.55 MeV helium ions in earth's outer magnetosphere ($L \sim 6$) using a novel technique. The radial gradient of the helium ion flux and the east-west anisotropy in the pitch-angle distribution are both measured. These are combined with measurements of the magnetic field to calculate the flux-weighted average ion gyroradius. Since the magnitude of the magnetic field and the energies of the ions are known, the gyroradius determines the ion's charge state. During two pairs - and		

DISTRIBUTION STATEMENT A

Approved for public release
Distribution UnlimitedDD FORM 1473
(FACSIMILE)

UNCLASSIFIED

SECURITY CLASSIFICATION OF THIS PAGE (When Data Entered)

UNCLASSIFIED

SECURITY CLASSIFICATION OF THIS PAGE(When Data Entered)

19 KEY WORDS (Continued)

20 ABSTRACT (Continued)

of geomagnetically quiet days in 1979 we find that most of these ions are singly charged. This result is in accord with theoretical calculations that find that charge-exchange reactions between these ions and the neutral hydrogen geocorona are the dominant factors in controlling the charge state of these ions at times longer than a day after their injection. Our results also suggest that the mean charge state of these helium ions may vary with position in the magnetosphere and with time.

UNCLASSIFIED

SECURITY CLASSIFICATION OF THIS PAGE(When Data Entered)

CONTENTS

INTRODUCTION.....	3
INSTRUMENTATION.....	5
METHOD OF ANALYSIS.....	7
RESULTS.....	17
DISCUSSION.....	21
REFERENCES.....	25

DTIC
ELECTE
NOV 16 1984
B

✓

A-1



FIGURES

1.	A cross-sectional diagram of The Aerospace's Corporation's heavy ion telescope aboard the SCATHA satellite.....	6
2.	An illustration of the "gradient cross B" anisotropy measurement technique.....	8
3.	The pitch angle distributions of helium ions observed in the dawn sector.....	9
4.	The pitch angle distribution of helium ions, sunward and anti-sunward directions averaged together (geometrically).....	12
5.	The radial distribution of the helium ion flux extrapolated to the magnetic equator, for two consecutive quiet days in the spring of 1979.....	13
6.	Same format as Figure 5, but for two days in the autumn of 1979.....	14

TABLE

1.	Radial gradient scale length, "average" charge state, and He^{++} abundance fraction.....	19
----	--	----

Introduction

The charge state of an energetic heavy ion in earth's magnetosphere can provide important information about the source of the ion and about the processes responsible for the formation and maintenance of the earth's radiation belts [Cornwall, 1972]. Helium ions are especially attractive candidates for charge state studies because these ions have only two charge states and because the mean charge states for the dominant magnetospheric ion sources are different. Ionospheric helium ions are dominantly He^+ , while solar wind helium is He^{++} [Axford, 1969]. Thus a measurement of the mean charge state of freshly injected helium ions can indicate the source of the ions. Blake et al. [1983] have exploited the timing of drift echos occasionally observed in the proton and helium fluxes to determine the charge state of the helium ions, which they found to be He^{++} , indicating freshly injected solar-wind plasma.

With increasing time after an injection, however, the effects of charge exchange will become the dominant factor in determining the observed charge state. If an energetic ion is neutralized by charge exchange, it is free to leave the magnetosphere. This loss is one of the important processes controlling the steady-state configuration of the heavy ion radiation belts. Also, the radial diffusion coefficient may depend on an ion's charge-to-mass ratio [Cornwall, 1972]. Thus, it is clear that the charge state of the energetic helium population is a fundamental parameter to be measured in studies of the radiation belts.

In this paper we present the first measurements of the quiet-time charge state distribution of stably trapped He ions with energies in the range 0.40 -

0.55 MeV. The charge state is determined by measuring the gyroradii of ions with a known kinetic energy. The gyroradius is determined by simultaneous measurements of the radial gradient of the ion flux intensity and of the east-west anisotropy in ion flux produced by the "radial-flux-gradient cross B" ($\nabla j \times \vec{B}$) effect. The magnitude of this anisotropy is proportional to the ratio between the ion gyroradius and the radial-flux-gradient scale length. These measurements were made near the equator in the outer zone, $5 < L < 7$, using The Aerospace Corporation's ion telescope aboard the SCATHA satellite [Blake and Fennell, 1981; Fennell, 1982].

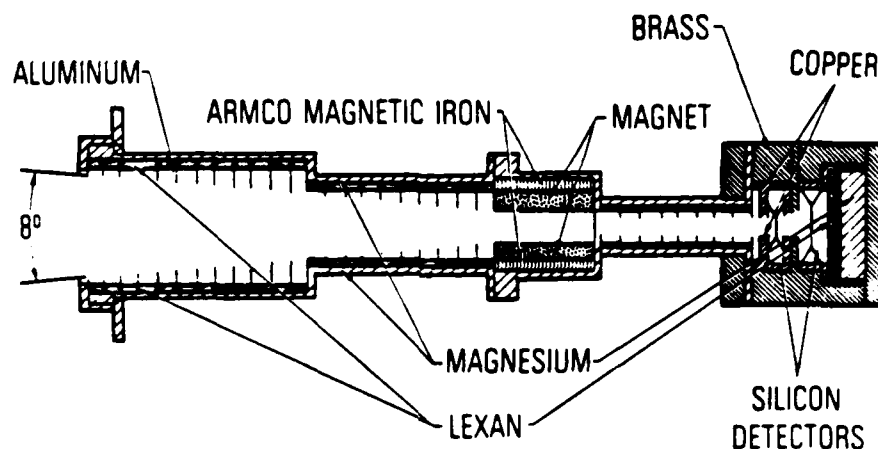
A preliminary report of these results was presented by Chenette et al. [1982]. These results complement the earlier work of Klecker et al. [1983] and Ma Sung et al. [1983] who have reported helium charge state measurements at somewhat higher energies.

Instrumentation

The Aerospace Corporation's ion telescope aboard SCATHA is a collimated two-detector range-energy telescope. It is illustrated in Figure 1. The rear detector, detector 2, is used to veto particles which penetrate detector 1. Detector 2 is operated with a threshold equivalent to 0.109 MeV energy deposit in the detector. Detector 1 is operated with six thresholds to separate He and heavier ions [Blake and Fennell, 1981]. The results presented in this paper are based on the lower energy He channel of this telescope, which counts incident He ions with energies from 0.40 to 0.55 MeV. This channel is used because its counting rates are high enough so that statistical uncertainties do not dominate the anisotropy signal being measured.

The data from the ion telescope consist of continuous 1-second samples of the counting rate of particles triggering a given threshold of detector 1 but not triggering detector 2. Each sample is assigned a pitch angle, which is the angle between the center of the detector field-of-view and the direction of the magnetic field measured simultaneously by the SCATHA magnetometer [Fennell, 1982].

SCATHA orbits between $L \sim 5.3$ and $L \sim 7.8$ with an inclination of 7.8° . The satellite spins at ~ 1 rpm and its spin axis is kept normal to the earth-sun line and directed from dusk to dawn. This orientation of the satellite generally permits instruments mounted perpendicular to the spin axis, like the ion telescope, to sample the full range of pitch angles every minute.



$$\text{GEOMETRIC FACTOR} = 3.6 \times 10^{-4} \text{ cm}^2 \text{ sr}$$

DETECTOR 1	2.3 microns, 10 mm ²
DETECTOR 2	42.1 microns, 25 mm ²

Figure 1. A cross-sectional diagram of The Aerospace Corporation's heavy ion telescope aboard the SCATHA satellite.

Method of Analysis

Figure 2 illustrates how the characteristics of the SCATHA satellite and its orbit allow us to make the measurements of the radial gradient and $\nabla j \times B$ anisotropy that are necessary for the present analysis. The radial gradient of these helium ions is directly measurable between 5.3 and 7.8 earth radii since SCATHA's orbit is eccentric although, because of the ~ 24 hour period of SCATHA, the L-range is covered only twice per day. Given that the dominant helium ion flux gradient is in the radial direction, the $\nabla j \times B$ anisotropy is measurable whenever the spin axis of the satellite has a significant radial component, e.g. near the dawn and dusk local time sectors. As Figure 2 illustrates, in the noon sector (and midnight) when the instrument views in the sunward and anti-sunward directions, ions are sampled whose gyrocenters are in roughly the same L-shell as the satellite. However, in the dawn sector, the telescope samples ions with gyrocenters at lower altitudes than the satellite when viewing sunward, and, when viewing anti-sunward, the telescope samples ions with gyrocenters at higher altitudes. Thus, since the ion flux near synchronous altitudes is more intense closer to earth, a net sunward anisotropy is observed. In the dusk sector, the direction of maximum of this component of the ion anisotropy will be anti-sunward. Since when viewing sunward and anti-sunward the telescope samples particles with gyrocenters separated by two gyroradii, the magnitude of this anisotropy is determined by both the particle's gyroradius and the spatial gradient of particle flux.

An example of this anisotropy is illustrated in Figure 3, where the pitch angle distributions measured in the sunward and anti-sunward directions are

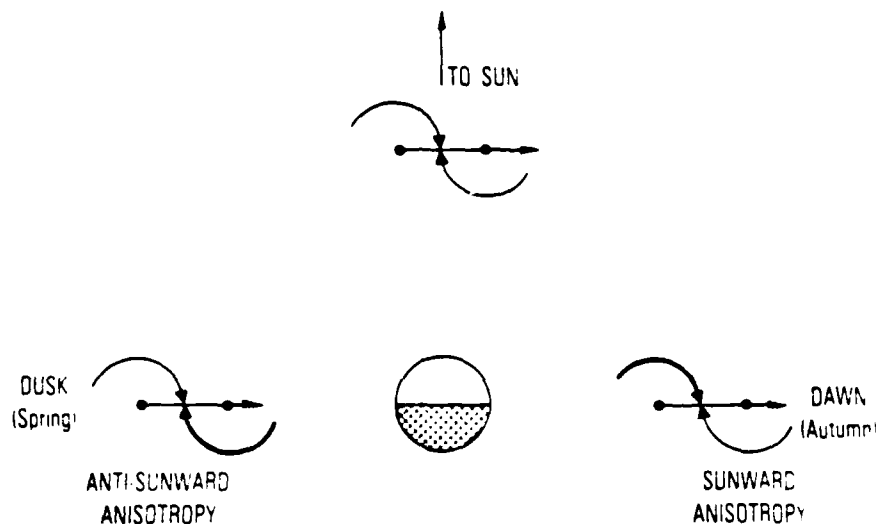


Figure 2. An illustration of the "gradient cross B" anisotropy measurement technique. Straight arrows pointing to the right indicate the SCATHA spin axis. Dots on those arrows are at gyrocenters of orbiting ions. At noon (and midnight) particles observed in the sunward and anti-sunward directions have gyrocenters at the same altitude. At dusk, the gyrocenters of ions observed in the anti-sunward (sunward) direction are inside (outside) the satellite orbit. Thus if the particle intensity is higher closer to the earth, a net anti-sunward anisotropy is observed. At dawn the direction of this anisotropy will be sunward.

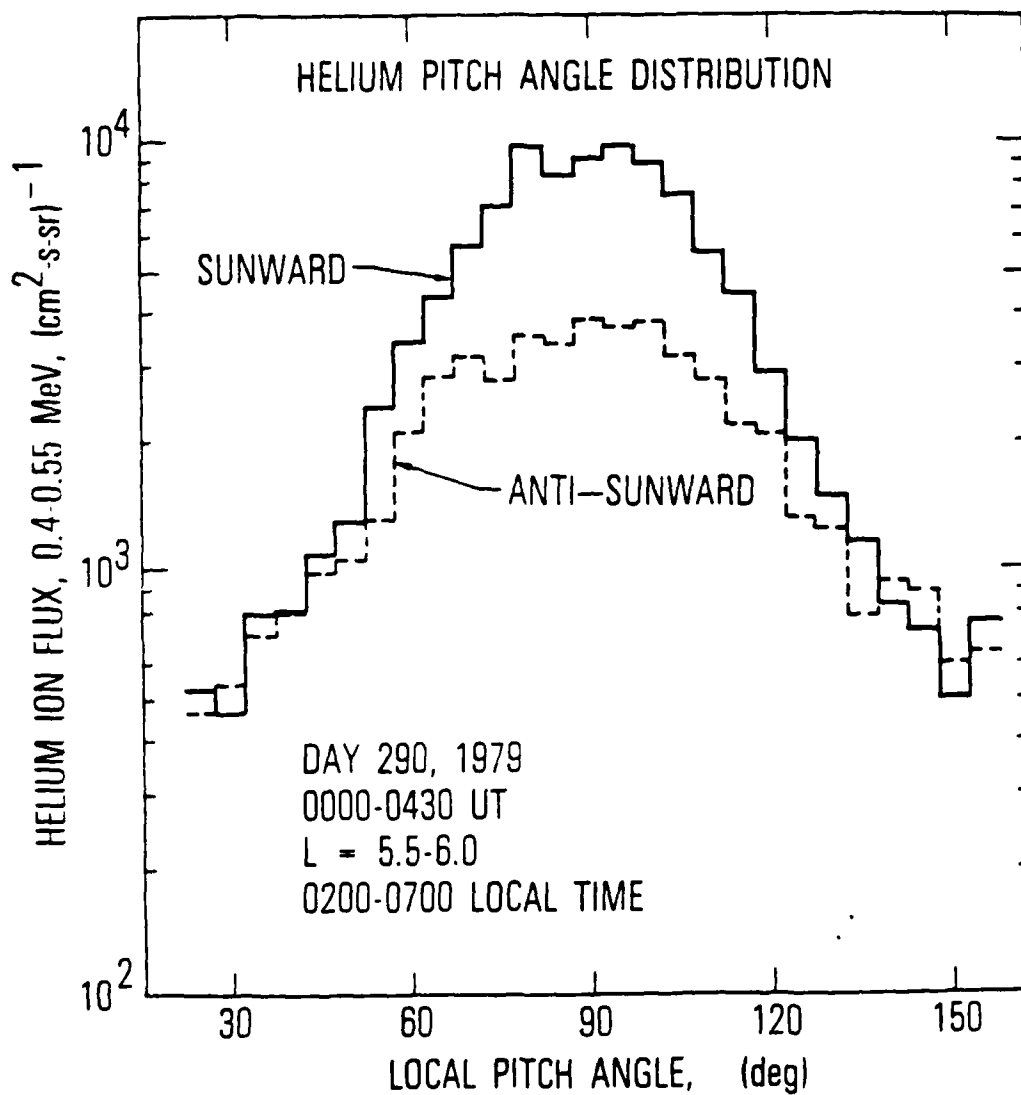


Figure 3. The pitch angle distributions of helium ions observed in the dawn sector. Sunward and anti-sunward directions are separated to show the "gradient cross B" anisotropy.

shown separately. The peak perpendicular flux in the sunward direction is ~ 2.5 times larger than the flux in the anti-sunward direction. If the radial profile of the helium flux were an exponential in magnetic L as $\exp(-L/L_0)$, then these data require $\exp(D/L_0) = 2.5$ or $D \sim L_0$, where D is the radial distance between the gyrocenters of ions sampled in the sunward and anti-sunward directions, respectively. If the SCATHA spin axis were aligned with the radial direction, then D would be equal to twice the ion gyroradius or

$$\frac{D}{2} = \rho_g = \frac{pc}{qB} \quad (1)$$

where p is the ion's momentum, c the speed of light, B is the local magnitude of the magnetic field, and q is the ion's charge. Since B is measured and p is known from the kinetic energy of the ion, q can be inferred by measuring both the anisotropy factor (2.5 in this case) and L_0 , the radial gradient scale length.

Since SCATHA's orbit is inclined relative to the magnetic equator, and since the pitch-angle distributions of these helium ions are anisotropic (Figure 3), the analysis of these data must be more sophisticated than outlined above. We have used the measured ion pitch angle distributions to calculate the perpendicular flux at the magnetic equator by assuming that these distributions are adequately represented by a function of the form

$$J(\alpha_0, L) = A \exp(-L/L_0) (\sin^2 \alpha_0)^Y \quad (2)$$

where L is the magnetic L-shell parameter and α_0 is the ion's equatorial pitch angle. The geometric mean of the sunward and anti-sunward flux is calculated at each L and these data are fit by a least-squares method to calculate the power-law index, γ . The geometric mean is used because it removes the dependence on L_0 in the model flux distribution.

Figure 4 illustrates a sample pitch angle distribution (sunward and antisunward data of Figure 3 averaged together geometrically) and the fit used to extrapolate the flux to the equator. This distribution exhibits two components: A steep inner component, fit as $\sin^{5.6} \alpha$, or $\gamma = 2.8$, and another, flatter component that is proportional to $\sin \alpha$ ($\gamma = 0.5$). This two component structure was observed throughout the periods that were analyzed. This effect has been discussed by Blake and Fennell [1981]. Thus to obtain reliable estimates of γ for our purposes, fits were restricted to the pitch-angle range 45° to 135° . For the periods that we analyzed, γ was typically in the range $2.5 < \gamma < 3.0$.

The data were corrected to the magnetic equator using γ and the measured magnetic field magnitude together with the minimum field magnitude on that field line obtained from the field model of Olsen and Pfitzer [1977]. L_0 was obtained from least-squares fits to these "corrected equatorial" data (Figures 5, 6). Only data obtained within 10° of the model magnetic equator have been used in this initial study to minimize the uncertainty introduced by extrapolations to the magnetic equator. For the present analysis, pitch angle distributions were averaged in contiguous 15-minute intervals.

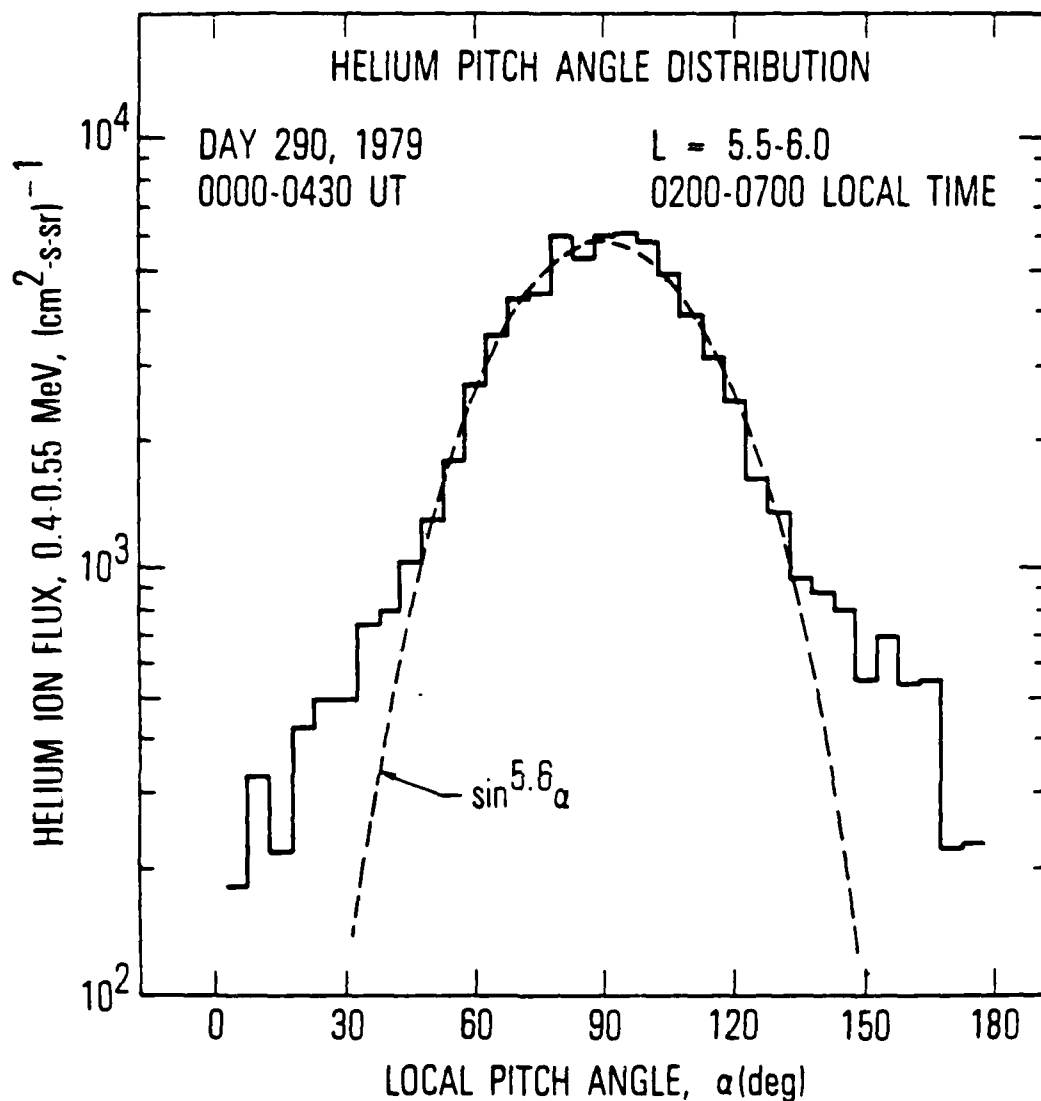


Figure 4. The pitch angle distribution of helium ions, sunward and anti-sunward directions averaged together (geometrically). The dashed line is the fit to the data over $45^\circ < \alpha < 135^\circ$ that was used to extrapolate the observations to the magnetic equator.

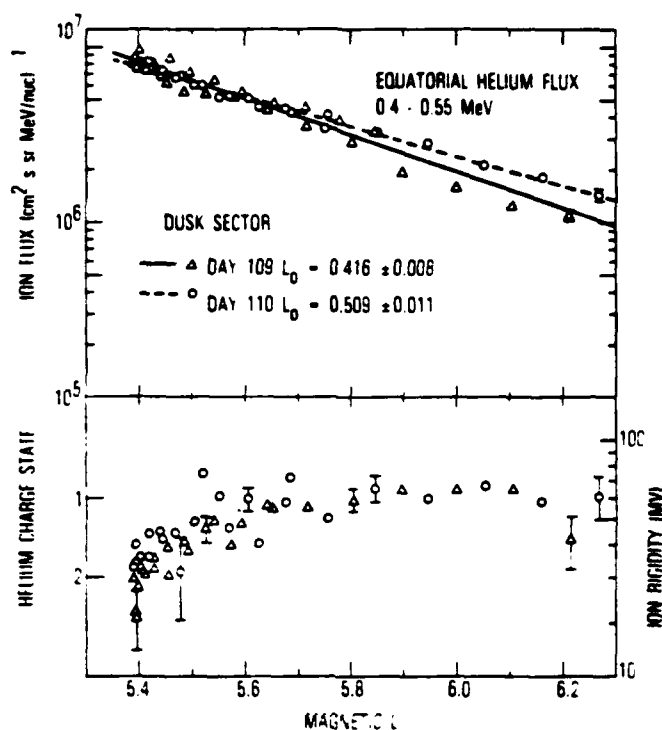


Figure 5. The radial distribution of the helium ion flux (upper panel) extrapolated to the magnetic equator, for two consecutive quiet days in the spring of 1979. Dashed and solid lines are exponential least-squares fits to these data with calculated e-folding scale length L_0 . The lower panel shows the "average" magnetic rigidity and helium charge state inferred from the "gradient cross B" anisotropy.

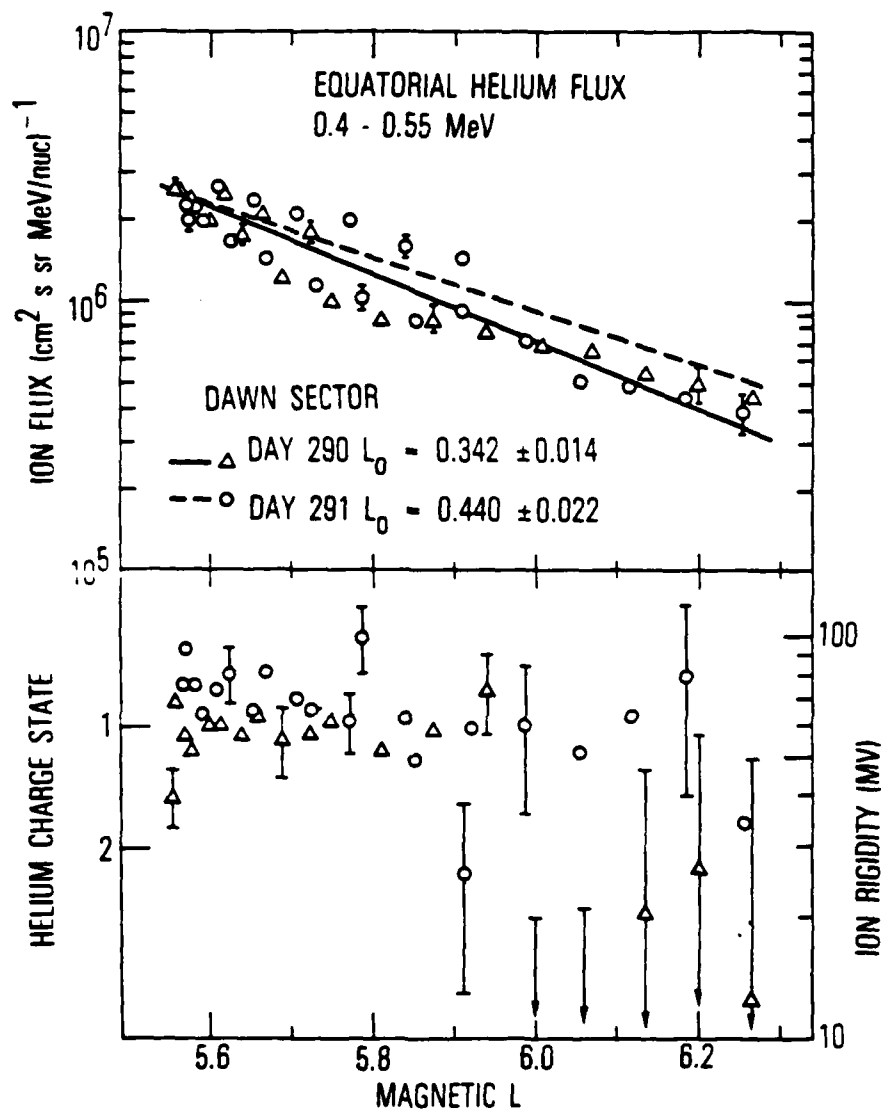


Figure 6. Same format as Figure 5, but for two days in the autumn of 1979.

To determine the helium ion charge state, we calculate the log ratio, W:

$$W = \frac{1}{2} \ln \left[\frac{J_s(90^\circ, L)}{J_a(90^\circ, L)} \right] \quad (3)$$

where $J_s(90^\circ, L)$ is the locally-mirroring ion flux in the sunward direction and $J_a(90^\circ, L)$ is the flux in the anti-sunward direction. If all of the ions have the same charge, q , then W is related to the ion gyroradius by

$$W = \rho_g \frac{\cos \theta}{L_0} \quad (4)$$

Thus the ion rigidity, R , may be calculated from W , L_0 , and the measured magnetic field, B , as

$$R = \frac{\sqrt{2MT}}{\langle q \rangle} = \frac{WB L_0}{\cos \theta} \quad (5)$$

In these relations, θ is the angle between the satellite spin axis and the radial direction (projected on a plane normal to B), M is the ion's mass, T its kinetic energy, and $\langle q \rangle$ is the "average" charge of the ion. If the helium flux is a mixture of charge states 1 and 2, then $\langle q \rangle$ will have a value between 1 and 2 but it will not be a flux-weighted average.

Results

The techniques described in the previous section were applied to two pairs of consecutive geomagnetically quiet days in the spring and autumn of 1979. Spring and autumn are preferred for this analysis because those are the times when SCATHA approaches minimum L in its orbit near dusk and dawn, respectively; thus the measured flux is larger and uncertainties due to counting statistics are minimized in the regions where the anisotropy signal is best measured. Quiet periods were studied in this initial analysis to reduce the confusion that would be introduced in the anisotropy and the radial gradient due to rapid temporal variations in flux intensity. The study was performed on two consecutive days in each season to measure the stability of the flux intensity from day to day as a monitor of temporal changes. The selected periods were: days 109 and 110 (April 19 and 20, 1979) and days 290 and 291 (October 17 and 18, 1979). These days were the geomagnetically quietest days in each of their respective months, with average geomagnetic activity amplitudes (A_p) of 6 and 2 on April 19 and 20, and $A_p = 4$ and 3 on October 17 and 18 [Lincoln, 1979; 1980].

The radial profile of the equatorial helium ion flux deduced from these SCATHA observations is plotted in the upper panels of Figures 5 and 6. These data were calculated from the pitch angle distributions measured off the equator and extrapolated to the equator using the methods described in the previous section.

For each day, data are included over the period surrounding the time the satellite reached minimum L in its orbit. SCATHA traversed a different range

of magnetic latitudes before and after this minimum L point. The scatter between adjacent flux points for each day reflects the error associated with the extrapolation of the flux to the equator because adjacent points are generally from different magnetic latitudes. This error is sometimes as much as 50%. However, the error induced in the radial gradient, which is the parameter of importance for the present study, is significantly smaller, as indicated in the figure. Representative error bars shown with the flux points in Figures 5 and 6 include only counting statistics uncertainties, not uncertainties, for example, due to deficiencies in the magnetic field model.

The lower panels of Figures 5 and 6 display the "average" ion rigidity, R (right scale), and "average" charge state, $\langle q \rangle$ (left scale), calculated from 15-minute averaged pitch angle distributions. The rigidity was calculated from the pitch angle distribution anisotropy using the values of L_0 from the upper panel for the day when the measurements were made. Representative error bars associated with some points include counting statistics uncertainties in the pitch angle distribution fits and the calculated uncertainty in L_0 . Since the instrument responds to helium ions with energies of 0.40 to 0.55 MeV, the mean momentum (p) used to convert from rigidity ($R = p/q$) to charge state (q) was $p = 59 \text{ MeV}/c$.

To account for the nonlinear weighting in the calculated average charge state $\langle q \rangle$, the results of Figures 5 and 6 are collected and averaged in contiguous L-bins. These averages are converted to the equivalent fractional abundance of He^{++} ($n(\text{He}^{++})/(n(\text{He}^+) + n(\text{He}^{++}))$), and are presented in Table 1.

Table 1. Radial gradient scale length, "average" charge state, and He^{++} abundance fraction

	L_0	*	$L = 5.3 - 5.5$	$L = 5.5 - 5.7$	$L = 5.7 - 5.9$	$L = 5.9 - 6.1$	$L = 6.1 - 6.3$
Day 109	0.416 ± 0.008	A	1.90 ± 0.19	1.26 ± 0.13	1.00 ± 0.11	0.91 ± 0.14	1.11 ± 0.17
		F	0.95 ± 0.05 $- 0.12$	0.41 ± 0.15 $- 0.18$	0 ± 0.20 $- 0$	0 ± 0.10 $- 0$	0.20 ± 0.24 $- 0.20$
Day 110	0.509 ± 0.011	A	1.53 ± 0.15	1.03 ± 0.10	1.03 ± 0.12	0.94 ± 0.12	0.99 ± 0.15
		F	0.69 ± 0.12 $- 0.14$	0.06 ± 0.17 $- 0.06$	0.06 ± 0.20 $- 0.06$	0 ± 0.12 $- 0$	0 ± 0.24 $- 0$
Day 290	0.342 ± 0.014	A	---	1.04 ± 0.10	1.03 ± 0.14	8 ± 19	1.8 ± 2.3
		F	---	0.08 ± 0.16 $- 0.08$	0.06 ± 0.23 $- 0.06$	---	---
Day 291	0.440 ± 0.022	A	---	0.79 ± 0.08	0.89 ± 0.10	1.46 ± 0.36	0.96 ± 0.37
		F	---	0	0	0.63 ± 0.27 $- 0.45$	0 ± 0.5 $- 0$

* A: "Average" charge state, non-linear weighting (Figures 5, 6)

F: Fractional He^{++} abundance = $\text{He}^{++}/(\text{He}^+ + \text{He}^{++})$

Discussion

The immediate conclusion to be drawn from Figures 5 and 6 and Table 1 is that the dominant charge state of the helium ions measured was $+1$. This result is qualitatively consistent with theoretical calculations of the equilibrium charge state of 400-keV helium ions in this region of the magnetosphere and it occurs because the $\text{He}^{++} + \text{He}^+$ charge exchange cross section is ~ 4 times larger than the $\text{He}^+ + \text{He}^{++}$ cross section at 400 keV in a neutral hydrogen atmosphere like the hydrogen geocorona [Tinsley, 1978; Spjeldvik and Fritz, 1978]. Extrapolation of the results presented by Tinsley [1976] suggests that the 400 keV He^{++} lifetime against charge exchange is only a few days at $L = 5$. This is much shorter than characteristic diffusion times in the quiet magnetosphere [Spjeldvik and Fritz, 1978; Klecker et al., 1983; Ma Sung et al., 1983, and references therein].

The data of Figure 5 and Table 1 also suggest that during the spring period (days 109 and 110) the relative abundances of He^+ and He^{++} varied spatially and with time. The spatial variation in the derived charge state could possibly be an artifact, due to a change in the radial gradient inside $L = 5.4$. Since the gyroradii of these ions in this region were nearly $0.2/q$ earth radii, where q is the ion charge, if the radial gradient of the flux were flatter between $L = 5.2$ and 5.4 than it was from $L = 5.4$ to 6.2 , a smaller ion gyroradius (higher charge state) would be inferred. There is no evidence in the available data to support this conjecture, however. To produce the significantly smaller average charge on the second day (110) would require the gradient inside the region traversed to become relatively steeper

at the same time that the observed gradient became flatter. Because the set of circumstances necessary to mimic this spatial variation is so artificial, we conclude that it is a real effect.

The temporal change in the relative abundances of He^+ and He^{++} on days 109 and 110 are in the direction that one would expect for an initial population of He^{++} evolving towards equilibrium via charge exchange. The charge exchange lifetimes for He^{++} inferred from these data are 3 ± 2 days for the $L = 5.3$ to 5.5 bin and < 1.3 days for the $L = 5.5$ to 5.7 bin. The latter value is somewhat smaller than expected [Tinsley, 1976; Spjeldvik and Fritz, 1978], but the dispersion of the measurements for day 110 between $L = 5.5$ and 5.7 is large and thus less confidence may be placed on results derived from these data.

The appearance on days 109 and 110 of a population of He^{++} ions within $L = 5.6$ which was decaying to He^+ suggests a scenario that will warrant further study; namely, that these He^{++} ions were directly injected and trapped in this region on the previous day. The radial transport of these He^{++} ions from their presumed source outside the magnetosphere to within $L = 5.6$ must have been faster than the charge exchange lifetime (a few days) and must have occurred only a fraction of this lifetime before the measurements were made on day 109. Thus studies of the helium-flux charge state provide a significant new channel of information for understanding magnetospheric dynamics.

The charge state measurements of $0.50 - 0.57$ MeV/nucleon helium ions have also been reported by Klecker et al. [1983] and Ma Sung et al. [1983]. The instrument used by these authors employs an electrostatic analyzer to

determine the ion's charge state directly. In this higher energy range He^{++} was the dominant ion during the intervals analyzed. This result is not inconsistent with the present analysis because at these higher energies the charge-exchange-equilibrium state is He^{++} rather than He^+ . However, Klecker et al. [1983] observed a localized peak in the $\text{He}^+/\text{He}^{++}$ ratio of ~ 0.4 at $L \sim 3.3$. They sought to explain this observation in terms of fast cross-L transport from the outer magnetosphere during magnetic storms. While the details of the processes necessary to produce the localized He^+ enhancement are unclear, this explanation depends on the existence of a He^+ population like that observed with the SCATHA instrument.

Finally, as Hovestadt et al. [1978] and Panasyuk [1980] have shown, the ion charge state plays a crucial role in determining whether and at what energies the ion can be trapped in the magnetosphere. Panasyuk [1980] determined, from laboratory model experiments, a relationship between the critical trapping energy E_{cr} , and the charge and mass of an ion (Q , M) as a function of L :

$$E_{\text{cr}}(\text{MeV}) = 2 \times 10^3 Q^2/M L^4 \quad (6)$$

At $L=6$ this critical energy is ~ 0.4 MeV for He^+ and ~ 1.5 MeV for He^{++} . Thus the charge exchange reaction $\text{He}^{++} + \text{He}^+$ will cause He ions in the energy range $0.4 - 1.5$ MeV to cross this critical energy threshold so that they may leave the magnetosphere. The SCATHA ion telescope is well-positioned in L and energy space to study the stable trapping limit for these ions.

Further analysis of the evolution of these particles, combined with charge state measurements, will provide more insight to the processes responsible for maintaining the heavy-ion population of the magnetosphere.

References

- Axford, W. I., On the origin of radiation belt and auroral primary ions, in Particles and Fields in the Magnetosphere, edited by B. M. McCormac, D. Reidel, Dordrecht, Netherlands, p. 46, 1970.
- Blake, J. B. and J. F. Fennell, Heavy ion measurements in the synchronous altitude region, Planet. and Sp. Sci., 29, 1205, 1981.
- Blake, J. B., J. F. Fennell, D. N. Baker, R. D. Belian and P. R. Higbie, A determination of the charge state of energetic magnetospheric ions by the observation of drift echos, Geophys. Res. Lett., 10, 1211, 1983.
- Chenette, D. L., J. B. Blake and J. F. Fennell, The magnetic rigidity and charge state of ≥ 0.4 MeV ions near $L = 6$, EOS, Trans. A. G. U., 63, 1078, 1982.
- Cornwall, John M., Radial diffusion of ionized helium and protons: A probe for magnetospheric dynamics, J. Geophys. Res., 77, 1756, 1972.
- Fennell, J. F., Description of P78-2 (SCATHA) satellite and experiments, in The IMS Source Book, edited by C. T. Russell and D. J. Southwood, American Geophysical Union, Washington, D. C., 1982.
- Hovestadt, D. G., Gloeckler, C. Y. Fan, L. A. Fisk, F. M. Ipavich, B. Klecker, J. J. O'Gallagher and M. Scholer, Evidence for solar wind origin of energetic heavy ions in the earth's radiation belts, Geophys. Res. Lett., 5, 1055, 1978.
- Klecker, B., D. Hovestadt, M. Scholer, G. Gloeckler, F. M. Ipavich and C. Y. Fan, Energy and charge distribution of energetic helium ions in the outer radiation belt of earth, J. Geophys. Res., 52, 239, 1983.

Lincoln, J. Virginia, ed., Geomagnetic and solar data, J. Geophys. Res., 84, 4472, 1979.

Lincoln, J. Virginia, ed., Geomagnetic and solar data, J. Geophys. Res., 85, 801, 1980.

Ma Sung, L. S., G. Gloeckler and D. Hovestadt, Ionization states of energetic helium ions in the earth's inner magnetosphere, EOS, Trans. A. G. U., 63, 1075, 1982.

Ma Sung, L., G. Gloeckler, D. Hovestadt and B. Klecker, Energetic He^+ and He^{++} in the earth's outer radiation belt, Proc. 18th Int. Cosmic Ray Conf., MG-5, 1983.

Olson, W. P. and K. A. Pfitzer, Magnetic field modeling, McDonnell Douglas Astronautics Company Annual Scientific Report to AFOSR, January, 1977.

Panasynk, M. I., Charge state of energetic radiation belt ions, Cosmic Research, 18, 64, 1980.

Spjeldvik, Walther N. and Theodore A. Fritz, Energetic ionized helium in the quiet time radiation belts: Theory and comparison with observation, J. Geophys. Res., 83, 654, 1978.

Tinsley, Brian A., Evidence that the recovery phase ring current consists of helium ions, J. Geophys. Res., 81, 6193, 1976.

LABORATORY OPERATIONS

The Laboratory Operations of The Aerospace Corporation is conducting experimental and theoretical investigations necessary for the evaluation and application of scientific advances to new military space systems. Versatility and flexibility have been developed to a high degree by the laboratory personnel in dealing with the many problems encountered in the nation's rapidly developing space systems. Expertise in the latest scientific developments is vital to the accomplishment of tasks related to these problems. The laboratories that contribute to this research are:

Aerophysics Laboratory: Launch vehicle and reentry aerodynamics and heat transfer, propulsion chemistry and fluid mechanics, structural mechanics, flight dynamics; high-temperature thermomechanics, gas kinetics and radiation; research in environmental chemistry and contamination; cw and pulsed chemical laser development including chemical kinetics, spectroscopy, optical resonators and beam pointing, atmospheric propagation, laser effects and countermeasures.

Chemistry and Physics Laboratory: Atmospheric chemical reactions, atmospheric optics, light scattering, state-specific chemical reactions and radiation transport in rocket plumes, applied laser spectroscopy, laser chemistry, battery electrochemistry, space vacuum and radiation effects on materials, lubrication and surface phenomena, thermionic emission, photosensitive materials and detectors, atomic frequency standards, and bioenvironmental research and monitoring.

Electronics Research Laboratory: Microelectronics, GaAs low-noise and power devices, semiconductor lasers, electromagnetic and optical propagation phenomena, quantum electronics, laser communications, lidar, and electro-optics; communication sciences, applied electronics, semiconductor crystal and device physics, radiometric imaging; millimeter-wave and microwave technology.

Information Sciences Research Office: Program verification, program translation, performance-sensitive system design, distributed architectures for spaceborne computers, fault-tolerant computer systems, artificial intelligence, and microelectronics applications.

Materials Sciences Laboratory: Development of new materials: metal matrix composites, polymers, and new forms of carbon; component failure analysis and reliability; fracture mechanics and stress corrosion; evaluation of materials in space environment; materials performance in space transportation systems; analysis of systems vulnerability and survivability in enemy-induced environments.

Space Sciences Laboratory: Atmospheric and ionospheric physics, radiation from the atmosphere, density and composition of the upper atmosphere, aurorae and airglow; magnetospheric physics, cosmic rays, generation and propagation of plasma waves in the magnetosphere; solar physics, infrared astronomy; the effects of nuclear explosions, magnetic storms, and solar activity on the earth's atmosphere, ionosphere, and magnetosphere; the effects of optical, electromagnetic, and particulate radiations in space on space systems.

. . .

END

UNFILMED

2-84

DTIC